

**NANOFRICTION PROPERTIES OF ULTRATHIN AMORPHOUS CARBON  
FILMS**

by

Jozef Mateusz Matlak

B.S. (University of California, Berkeley) 2011

A report submitted in partial satisfaction of the  
requirements for the degree of

Masters of Science, Plan II

in

Mechanical Engineering

at the

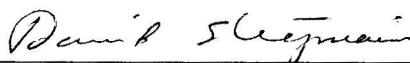
University of California at Berkeley

Committee in charge:



---

Professor Kyriakos Komvopoulos, Chairman



---

Professor David Steigmann

Spring 2014

**NANOFRICTION PROPERTIES OF ULTRATHIN AMORPHOUS CARBON  
FILMS**

Copyright 2014

by

Jozef Mateusz Matlak

**Abstract**

## NANOFRICTION PROPERTIES OF ULTRATHIN AMORPHOUS CARBON FILMS

by

Jozef Mateusz Matlak

Masters of Science, Plan II in Engineering-Mechanical Engineering

University of California, Berkeley

Professor Kyriakos Komvopoulos, Chair

The dependence of frictional properties of ultrathin amorphous carbon (*a*-C) films deposited on Si(100) substrates by radio frequency sputtering and filtered cathodic vacuum arc on their nanomechanical and structural properties was investigated using surface force microscopy. Deposition parameters promoting high  $sp^3$  content films were used to produce films with thickness ranging between 5 - 35 nm. The friction properties of the films were determined with a 1  $\mu\text{m}$  radius conical diamond tip. The coefficient of friction of the *a*-C films was found to be influenced by the film's nanomechanical properties, bonding type, thickness, and surface roughness. The dependence of the coefficient of friction on contact load and the dominant friction mechanisms of elastically and plastically deformed films are discussed with new insight into the intermixing layers within the ultrathin films.

# Contents

|                                  |            |
|----------------------------------|------------|
| <b>Contents</b>                  | <b>i</b>   |
| <b>List of Figures</b>           | <b>ii</b>  |
| <b>List of Tables</b>            | <b>iii</b> |
| <b>1 Introduction</b>            | <b>1</b>   |
| 1.1 Background . . . . .         | 1          |
| <b>2 Experimental Procedures</b> | <b>13</b>  |
| 2.1 Film deposition . . . . .    | 13         |
| 2.2 Characterization . . . . .   | 16         |
| <b>3 Results</b>                 | <b>21</b>  |
| <b>4 Discussion</b>              | <b>27</b>  |
| <b>5 Conclusions</b>             | <b>30</b>  |
| <b>References</b>                | <b>31</b>  |

# List of Figures

|     |  |    |
|-----|--|----|
| 1.1 | Schematic of (a) hard-drive disk layout showing only the disk and the read/write magnetic head and (b) cross-sectional view showing the layers of the hard disk. .   | 3  |
| 1.2 | Schematics of (a) top and (b) front views of the FCVA system. Four raster coils attached to the outside of the downstream coil (omitted from diagram) are used to direct the plasma toward the substrate holder. . . . .                   | 8  |
| 1.3 | Schematic of the RF system showing main components. . . . .  | 12 |
| 2.1 | (a) FCVA and (b) RF sputtering systems used for deposition of <i>a</i> -C films (Surface Science and Engineering Laboratory, Etcheverry Hall, Berkeley, CA). . . . .   | 14 |
| 2.2 | Hysitron Triboscope <sup>®</sup> system used for mechanical characterization of <i>a</i> -C films.   | 17 |
| 2.3 | Schematic of the scanning force microscope. . . . .  | 18 |
| 3.1 | Surface roughness of FCVA and RF sputtered films of varying thickness. . . . .   | 22 |
| 3.2 | Roughness profiles of FCVA deposited films with thickness (a) 6-7 nm, (b) 10 nm, (c) 20 nm, and (d) 35 nm. . . . .   | 23 |
| 3.3 | Roughness profiles of RF deposited films with thickness (a) 5 nm, (b) 10 nm, (c) 20 nm, and (d) 35 nm. . . . .   | 24 |
| 3.4 | Coefficient of friction across a 10 $\mu$ m scratch track for FCVA films of thickness (a) 5 - 7 nm, (b) 10 nm, (c) 20 nm, and (d) 35 nm, and RF sputtered films with thickness, (e) 5 - 7 nm, (f) 10 nm, (g) 20 nm, and (h) 35 nm. . . . . | 25 |
| 3.5 | Steady state coefficient of friction for various loads for FCVA and RF sputtered films with thickness (a) 5 - 7 nm, (b) 10 nm, (c) 20 nm, and (d) 35 nm. . . . .   | 26 |

# List of Tables

|     |   |    |
|-----|---|----|
| 1.1 | Common deposition methods and the properties of carbon films deposited by them. | 5  |
| 2.1 | Deposition parameters and thickness of FCVA <i>a</i> -C films. . . . .          | 15 |
| 2.2 | Deposition parameters and thickness of RF sputtered <i>a</i> -C films. . . . .  | 16 |

## Acknowledgments

I would like to thank my research advisor, Professor K. Komvopoulos, who has provided much encouragement, inspiration, and guidance throughout my research work. Furthermore, I would like to express my gratitude to my brother, Tomasz Matlak, and my parents, Jozef Matlak and Danuta Matlak, who have continuously supported me in all of my academic endeavors.

Funding of this work by the Computer Mechanics Laboratory (CML) and the UC Berkeley - KAUST Academic Excellence Alliance (AEA) Program is acknowledged.

# Chapter 1

## Introduction

### 1.1 Background

Significant interest in amorphous carbon (*a*-C), or diamond-like carbon (DLC), films has been generated due to their combination of desirable properties important in several tribological, biomedical, and electronic applications. This includes high hardness, friction and wear resistance, chemical inertness, low magnetic susceptibility, as well as a large optical band gap. Several techniques for synthesizing carbon films have been developed including radio frequency (RF) sputtering, ion-beam deposition, laser ablation, and filtered cathodic vacuum arc (FCVA). Depending on the deposition method and parameters employed, the structure of the film, including its uniformity, roughness, and bonding configurations, will vary, and influence the films overall quality. The industrial relevance of thin films, especially in the hard drive disk industry, makes the characterization of thin films imperative. An



investigation of the tribological properties including friction and roughness of thin *a*-C films deposited with both FCVA and RF Sputtering systems will be made and the results will be interpreted with new insight into the intermixing layers of the films.

### 1.1.1 Applications

A prominent application of *a*-C films is in magnetic storage devices where maintaining the integrity of data is of crucial importance [1, 2, 3]. In such devices, information is recorded in a layer of a ferromagnetic material (typically, Co Cr Pt) through the application of a magnetic field induced by a transducer located at the trailing edge of the flying magnetic head, as shown in Figure 1.1.

Ultrathin layers of *a*-C are deposited on both the disk and head to protect against impact, wear, and corrosion, and, in turn, preserve the reliability of the storage device [4, 5]. A lubricant monolayer adsorbed onto the carbon layer further provides additional protection and helps decrease adhesion between the magnetic head and the hard disk.

Since data storage density increases exponentially with decreasing magnetic spacing, the overcoat thickness is usually no more than several nanometers to ensure minimal physical spacing between the read/write transducer and the magnetic medium. With a film thickness less than a few nanometers, storage densities may be increased from several hundreds of Gbit/in<sup>2</sup> to several Tbit/in<sup>2</sup> [6]. Efforts to reduce the thickness of the protective *a*-C layer below a few nanometers while preserving mechanical and tribological properties and

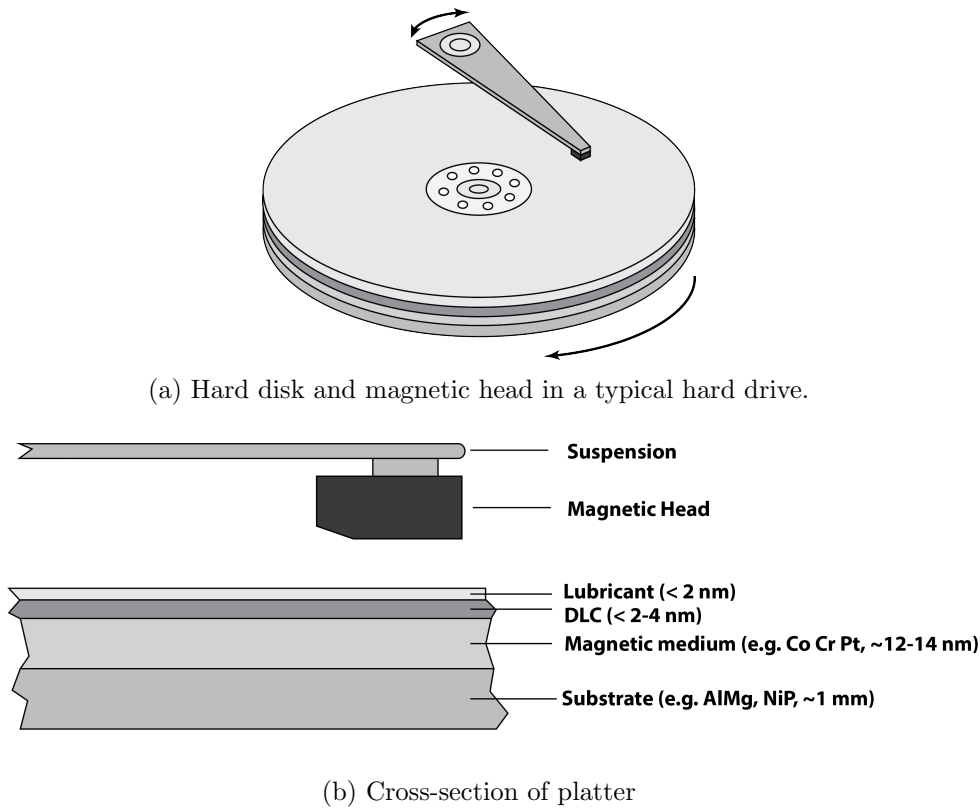


Figure 1.1: Schematic of (a) hard-drive disk layout showing only the disk and the read/write magnetic head and (b) cross-sectional view showing the layers of the hard disk.

preventing corrosion is thus challenging and of significant technological importance.

### 1.1.2 Materials

The structure of  $a$ -C films consists of short-range order of carbon atoms in three bonding configurations:  $sp^1$ ,  $sp^2$ , and  $sp^3$ . The  $sp^2$  and  $sp^3$  hybridizations form graphite-like and diamond-like carbon (DLC) bonding, respectively, where  $sp^2$  consists of both  $\sigma$  and  $\pi$  bonds, while  $sp^3$  only consists of  $\sigma$ -bonds. The stronger  $\sigma$ -bonds have been found to primarily influence mechanical properties, while the weaker  $\pi$ -bonds generally influence electrical and

optical properties [3, 7]. Films that have higher hardness, typically denoted as DLC films, tend to have higher  $sp^3$  content which usually is an indicator of better film protection against mechanical wear [8, 9]. DLC films are furthermore covalently bonded and generally form a metastable amorphous network with a micro- or nano-crystalline phase exhibiting various levels of intermediate-range ordering.

The films are typically deposited on Si, Fe, and Ti substrates where the formation of carbides in the intermixing layer of the film creates a strong adhesion between the film and the substrate. Adequate adhesion of the films to other substrates usually requires an interlayer of silicon by the majority of deposition methods. Post-processing of the films is generally not required, as the films tend to replicate the substrate topography.

### 1.1.3 Deposition Methods

Several deposition methods are used for the formation of ultrathin  $a$ -C films including filtered cathodic vacuum arc (FCVA) [9, 10], pulsed laser deposition [9, 11], chemical vapor deposition [9, 12], and radio frequency (RF) sputtering [13]. A summary of the mechanical and friction properties of films produced by these deposition systems is given in Table 1.1. The structure and corresponding mechanical properties of the films vary by deposition process and individual process parameters (e.g., substrate bias voltage, plasma power, ion fluence and incidence angle) [1, 2, 3, 10].

Both mechanical and tribological properties of carbon films can be correlated to the

$sp^3/sp^2$  bonded carbon ratio, hydrogen content, and the adhesion of the film to the substrate, which are all influenced by the deposition method. Generally, a higher fraction of  $sp^3$  hybridization in  $a$ -C films corresponds to a higher hardness [16]. The  $sp^3/sp^2$  ratio generally decreases in the following order: filtered cathodic vacuum arc deposition, pulsed laser vaporization, direct ion-beam deposition, plasma-enhanced chemical vapor deposition, ion-beam sputtering, and sputtering [14, 15, 16]. Previous investigations have shown that a kinetic energy of at least 100 eV is needed to achieve the formation of sufficiently high  $sp^3$  bonded carbon.

The remainder of this report will primarily focus on both FCVA and RF Sputtering, two industrially relevant deposition processes.

Table 1.1: Common deposition methods and the properties of carbon films deposited by them.

| Deposition Method   | Deposition Rate (nm/s) <sup>[17]</sup> | Kinetic Energy (eV) <sup>[17]</sup> | Hardness (GPa)        | Elastic Modulus (GPa)    | Friction Coefficient    |
|---|--|-------------------------------------|-----------------------|--------------------------|-------------------------|
| Filtered Cathodic Vacuum Arc (FCVA)                                     | 0.1-1                                  | 100-2500                            | 80 <sup>[4,5]</sup>   | 700-800 <sup>[4,5]</sup> | 0.1-0.2 <sup>[6]</sup>  |
| Direct Ion Beam (IB)  | 0.1-1                                  | 50-500                              | 10-40 <sup>[18]</sup> | -                        | 0.1-0.2 <sup>[18]</sup> |
| Plasma-Enhanced Chemical Vapor Deposition (PECVD)                       | 1-10                                   | 1-50                                | 33-35 <sup>[19]</sup> | -200 <sup>[19]</sup>     | -                       |
| Electron Cyclotron Resonance Plasma Chemical Vapor Deposition (ECR-CVD) | 1-10                                   | 1-10                                | -                     | -                        | -                       |
| DC/RF Sputtering  | 1-10                                   | 1-10                                | 10-45 <sup>[20]</sup> | 100-200                  | 0.1-0.3                 |

## Filtered Cathodic Vacuum Arc

FCVA deposition is a promising technique that enables low temperature deposition of carbon films with high  $sp^3$  content on various substrates without the need of an adhesion underlayer. The advantages of FCVA include the ability to deposit continuous ultrathin  $a$ -C films less than a few nanometers thick, while maintaining exceptionally high hardness and low surface roughness. The primary disadvantages of this technique have been plasma instabilities, difficulties with macroparticle filtering, and poor adhesion on electrically insulating substances [17]. However, many technical improvements, especially to the filtering process, have alleviated many of these issues.

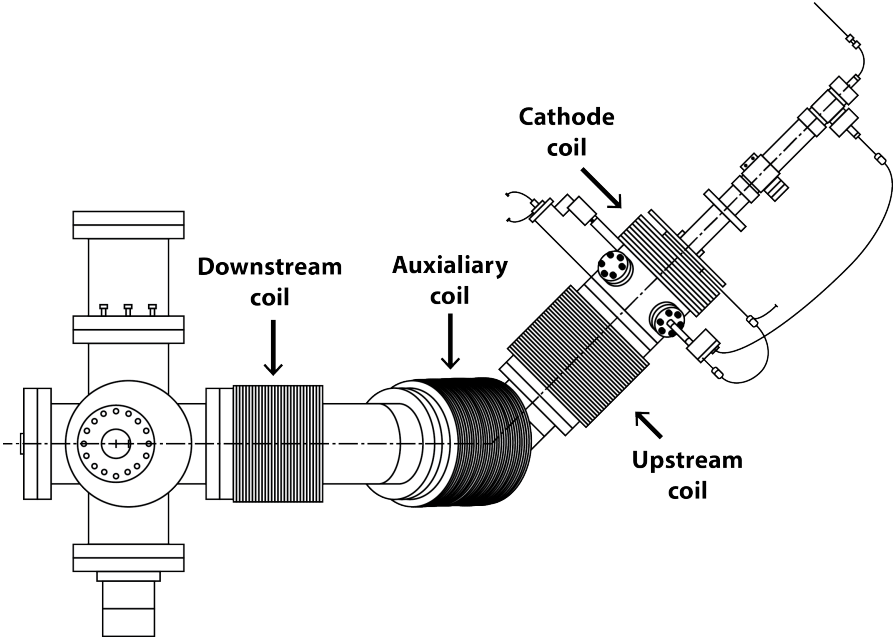
**Theory** Classified as a physical vapor deposition technique, FCVA uses a vacuum arc plasma source to deposit a film onto a substrate. The process relies on the ignition of a vacuum electric arc between the anode and the cathode (typically a high purity material - any element of the periodic table). The flow of electrons from the cathode during arc discharging creates both a pressure and electrical potential gradient, which refocuses the arc onto fluctuating small spots on the cathode surface. This creates pressurized gradients close to the cathode surface, resulting in the ejection of cathodic material in the form of plasma.

There are two types of modes for cathodic vacuum arc discharge: pulsed arc and direct current (DC) arc. High-frequency pulsed arcs can be used to reduce plasma instabilities though can result in significant reduction in deposition rates. Furthermore they add addi-

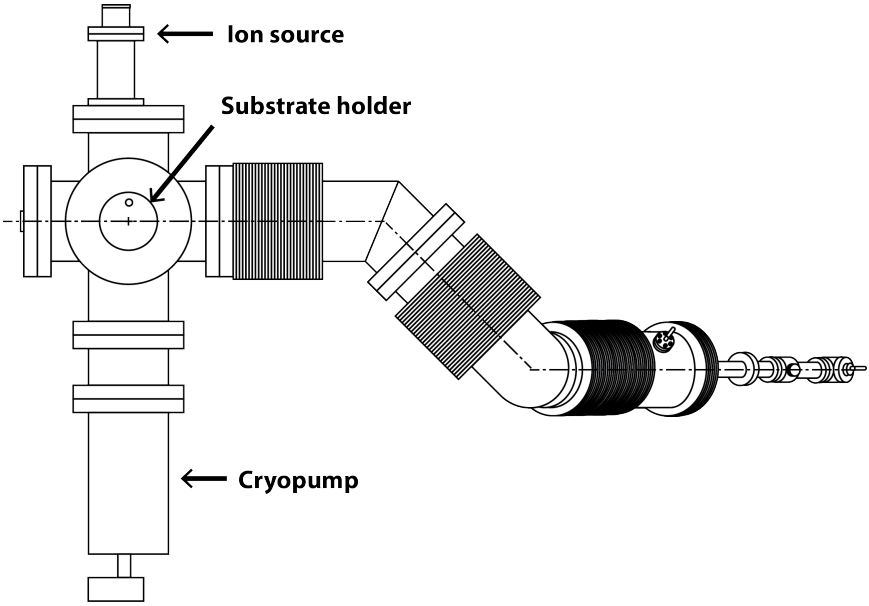
tional complexity by requiring in-phase coupling of the arc pulse and substrate bias pulse. DC arcs enable higher deposition rates but cause plasma instabilities during arc discharge due to a movement of arching spots toward the edge of a cathode surface. The addition of a magnetic field to a DC system, can, however, stabilize DC arc discharge [21]. Such a system was used to deposit the films examined in this study.

**Equipment** The FCVA samples examined in this study were fabricated using the system shown schematically in Figure 1.2. The process begins with plasma generation at the 99.99% pure graphite cathode between the cathode and the upstream anode. The plasma is then guided through the upstream, auxiliary, and downstream coils towards a rotating substrate holder to ensure uniform deposition. Four orthogonally mounted raster coils positioned outside the downstream coil raster the plasma beam. Water cooling is employed to remove excess heat generated at the cathode and substrate holder. The base chamber is pressured with a cryopump to less than  $10^{-7}$  Torr. Prior to film deposition, the substrate is cleaned with  $\text{Ar}^+$  ion bombardment using a 64 mm Kaufman ion source [21].

To stabilize the DC arc discharge configuration and arc discharge current, a relatively high strength and novel configuration of magnetic field is created through the superposition of the magnetic fields generated by the cathode coil and the upstream anode coil [21]. The ‘S-shaped’ duct configuration, which is the three-dimensional configuration of the magnetic filter, helps prevent macroparticle and/or droplets that may be ejected from the cathode from depositing onto the film surface.



(a) Top view of FCVA system.



(b) Front view of FCVA system.

Figure 1.2: Schematics of (a) top and (b) front views of the FCVA system. Four raster coils attached to the outside of the downstream coil (omitted from diagram) are used to direct the plasma toward the substrate holder.

The flow direction and the energy of the film can be controlled by adjusting the magnetic and electrical fields, respectively. A magnetic or electrical plasma filter is installed to remove macroparticles of cathode material that also form during arc discharging.

**Deposited Films** Film quality of FCVA-deposited *a*-C films is strongly correlated to the  $C^+$  ion energy and substrate bias voltage. An increase in ion energy results in intense collisions between  $C^+$  ions and substrate atoms, promoting  $sp^3$  hybridization. Too high of an ion energy, however, can also result in thermal relaxation and  $sp^3$  to  $sp^2$  rehybridization [22]. An optimal  $C^+$  ion energy, determined to be  $\sim 120$  eV [18], is therefore used to balance these opposing processes and maximize the  $sp^3$  fraction and film nanohardness [22].

### Radio Frequency Sputtering

Radio-Frequency (RF) sputtering is a technique that enables fast deposition of carbon films. The advantages of RF include the ability to deposit films under lower pressures than FCVA, which results in less gas collisions and increased line of sight deposition. Reversing polarity furthermore prevents charge-up effects and reduces arcing. Unlike FCVA, RF sputtering cannot produce continuous thin films less than 5 nm thickness due to clustering of carbon atoms into small islands prior to coalescing to form a continuous film. The  $sp^3$  content of RF sputtered films also tends to be notably less than that of FCVA films, resulting in films with relatively lower hardness.



**Theory** Classified as a physical vapor deposition technique, RF sputtering involves ejecting matter from a target onto a substrate. The process is initiated in a glow discharge produced in a vacuum chamber under pressure-controlled gas flow. An inert gas such as argon, neon, or krypton is used depending on the cohesive energy of the target. A power source generates radio frequency waves to ionize the gas atoms which then bombard the target material. With sufficient ion energy, the resulting momentum transfer expels atoms from the target surface, which then travel through the plasma and deposit onto the substrate surface to form a thin film.

Since individual atoms are chemically active, the inert gas helps prevent the formation of undesirable compounds. When the ions bombard the target, their electrical charge is neutralized. Assuming an insulated target, this process will result in a positive charge on the target surface. With enough charge build up, subsequent impacting ions may be repelled away and the sputtering process will halt. To avoid charge build up, radio frequency is employed where the application of a RF voltage onto the target assembly can reverse the polarity by attracting enough electrons from the discharge to neutralize charge build up.

**Equipment** The RF sputtered samples examined in this study were fabricated using the system schematically shown in Figure 1.3. Carbon material is sputtered from a graphite target with  $\text{Ar}^+$  plasma. The energetic ion bombardment, controlled by the biased substrate voltage, is used to enhance the film density and hardness of the growing film by resputtering the weakly bonded carbon atoms. During deposition, the base chamber is pressured with a

cryopump to less than  $10^{-6}$  Torr. Prior to film deposition, the substrate is cleaned with an etching process using Ar.

**Deposited Films** Film quality of RF-deposited *a*-C films is strongly correlated to the RF power and substrate bias voltage. An optimal forwarded RF power of 750 W and substrate bias voltage of -200 V was found to maximize hardness and elastic modulus, while minimizing friction and roughness. Under these conditions, the impinging ions effectively eliminate the weak carbon bonds while minimizing damage to the film microstructure.

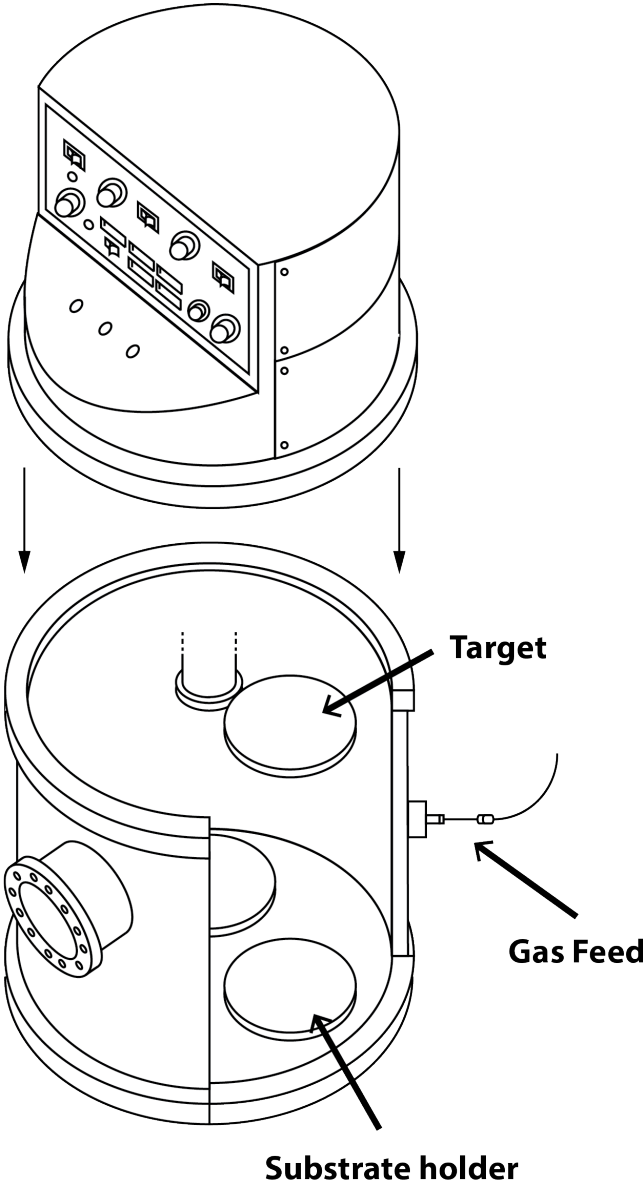


Figure 1.3: Schematic of the RF system showing main components.

## Chapter 2

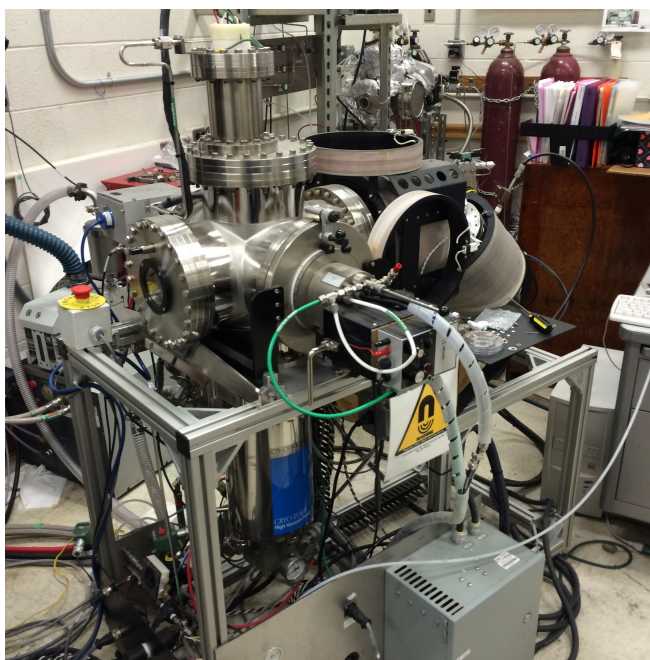
# Experimental Procedures

### 2.1 Film deposition

Thin amorphous carbon films with thicknesses ranging between 5 and 35 nm were prepared using both the FCVA and RF sputtering systems shown in Figure 2.1. Each system was configured with deposition parameters that were conducive to maximizing  $sp^3$  content. The procedure for each system is outlined in the following sections.

#### 2.1.1 FCVA

Substrate samples ( $10 \times 10 \text{ mm}^2$ ) were cut from  $p$ -type Si(100) wafers, rinsed in isopropanol followed by acetone for 10 min each, and then blow dried with nitrogen gas. After mounting the samples onto a substrate holder, the FCVA chamber was pumped down to a base pressure of  $<5 \times 10^{-7}$  Torr. The introduction of Ar gas raised the pressure to  $2 \times 10^{-4}$



(a) FCVA System



(b) RF Sputtering System (Perkine-Elmer Randex-2400 model)

Figure 2.1: (a) FCVA and (b) RF sputtering systems used for deposition of *a*-C films (Surface Science and Engineering Laboratory, Etcheverry Hall, Berkeley, CA).

Torr. To remove the native SiO<sub>2</sub> layer, Ar<sup>+</sup> ion sputter etching was performed for 2 min at 500 eV of power. The incidence angle of bombarding Ar<sup>+</sup> ions was set to 60° relative to the normal of the substrate surface. During deposition, a base pressure of  $<5 \times 10^{-7}$  Torr was maintained, and carbon plasma was formed by arcing on the cathode surface. This process was stabilized by a cusp-configuration magnetic field applied to the cathode. A pulsed bias voltage of -100 V at 25 kHz frequency was applied to the substrate. For each film deposited, varying deposition times were set to achieve the desired thickness. The deposition parameters for the examined FCVA films in this study are shown in Table 2.1.

Table 2.1: Deposition parameters and thickness of FCVA *a*-C films.

| <b>Film thickness (nm)</b> | <b>Incident angle (deg.)</b> | <b>Substrate bias (V)</b> | <b>Deposition time (s)</b> |
|----------------------------|------------------------------|---------------------------|----------------------------|
| 6-7                        | 20                           | -100                      | 30                         |
| 10                         | 10                           | -100                      | 12                         |
| 20                         | 45                           | -100                      | 30                         |
| 35                         | 90                           | -100                      | 30                         |

### 2.1.2 RF Sputtering

Substrate samples ( $10 \times 10 \text{ mm}^2$ ) were cut from *p*-type Si(100) wafers and rinsed in isopropanol followed by acetone for 10 min each, and then blow dried with nitrogen gas. The deposition procedure involved pumping down the RF chamber to a base pressure of  $<5 \times 10^{-6}$  Torr. Ar gas was introduced at a mass flow rate of 20 sccm into the chamber. The chamber pressure was raised to 3 mTorr by adjusting the throttle valve. Prior to each

film deposition, the graphite target was sputtered cleaned for 10 minutes and the Si(100) substrate was sputter etched for 3 min to remove the native SiO<sub>2</sub> layer. Both of these processes were performed at 250 W RF power and 3 mTorr working pressure in pure Ar plasma. The self-biased target voltage ranged from -750 to -850 V during cleaning of the substrate surface, and -980 to -1000 V when cleaning the target. During film deposition, a substrate bias of -200 V and forward RF power of 750 W were set to promote deposition of films with high hardness, low roughness, and a high  $sp^3$  fraction. Deposition times were varied to obtain films with the desired thickness. The deposition parameters for the RF sputtered films examined in this study are shown in Table 2.2.

Table 2.2: Deposition parameters and thickness of RF sputtered *a*-C films.

| <b>Film thickness (nm)</b> | <b>Forwarded RF power (W)</b> | <b>Substrate bias (V)</b> | <b>Target bias (V)</b> | <b>Deposition time (s)</b> |
|----------------------------|-------------------------------|---------------------------|------------------------|----------------------------|
| 5                          | 750                           | -200                      | -1500                  | 30                         |
| 10                         | 750                           | -200                      | -1480                  | 60                         |
| 20                         | 750                           | -200                      | -1400                  | 120                        |
| 35                         | 750                           | -200                      | -1500                  | 210                        |

Working pressure = 3 mTorr; Ar gas flow rate = 20 sccm

## 2.2 Characterization

Nanomechanical properties including hardness, elastic modulus, and coefficient of friction were obtained using a nanoindenter/scratcher while tribological properties such as roughness were measured using an Atomic Force Microscope (AFM).

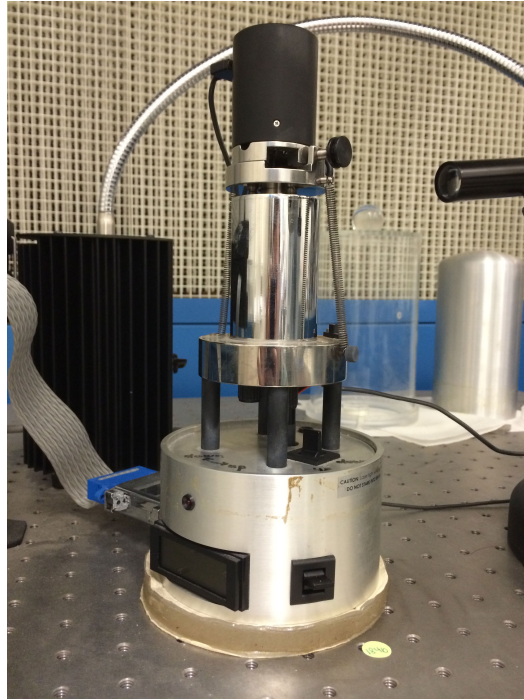


Figure 2.2: Hysitron Triboscope <sup>®</sup> system used for mechanical characterization of *a*-C films.

### 2.2.1 Nanomechanical testing

Nanomechanical properties of the deposited films were obtained using a scanning force microscope (SFM) consisting of a Digital Instruments Nanoscope II <sup>®</sup> AFM retrofitted with a Hysitron Triboscope <sup>®</sup> capacitive force transducer as shown in Figure 2.2. The transducer, shown schematically in Figure 2.3, consists of three-plate capacitors that enable highly sensitive vertical and lateral displacement and force measurements. An AFM controller and transducer controller are part of a computer workstation used for both operation of the equipment and for data acquisition. A control unit provides a force readout as well as offset, gain control, and filtering of the microscope z-feedback.



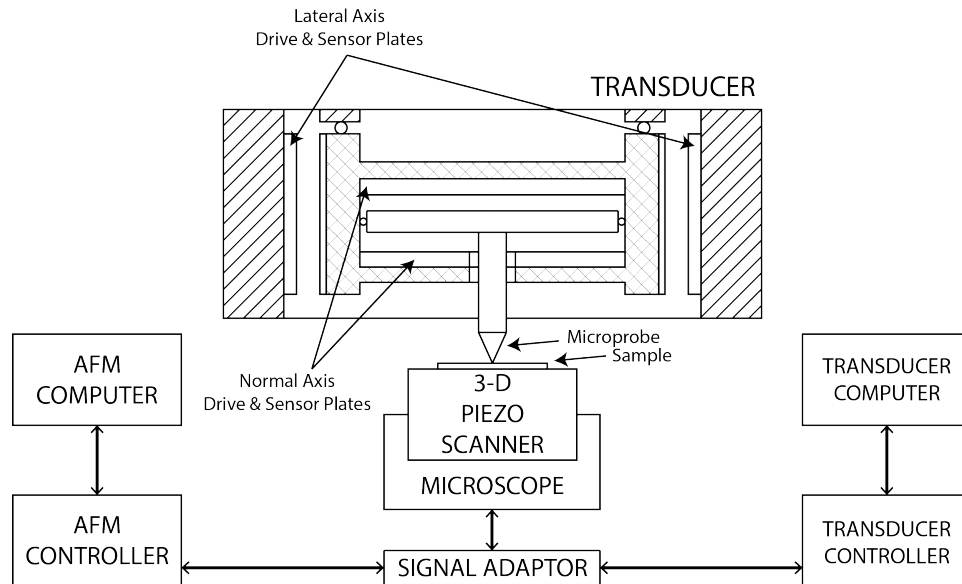


Figure 2.3: Schematic of the scanning force microscope.

A  $1\ \mu\text{m}$  conical diamond tip was attached to the transducer and used for all indentation and tribological tests. To relate the contact area of the tip to its indentation depth, a polynomial tip-shape function was derived by following a tip calibration procedure. This involved performing several indentations on a smooth fused quartz standard sample with a hardness of 10 GPa and in-plane (reduced) elastic modulus of 69.6 GPa. As the tip may physically deform after testing, the tip calibration procedure was repeated frequently in order to maintain an accurate tip-shape function.

To obtain the hardness and in-plane elastic modulus of the tested samples, the indentation (contact) depth at maximum load and the slope of the unloading portion of the indentation curve was determined from the recorded force-displacement material response. Hardness was calculated as the ratio of the maximum applied indentation load to the projected contact

area, as determined from the polynomial tip-shape function at the corresponding indentation depth [23]. The reduced elastic modulus was derived from the stiffness obtained from the slope of the unloading curve at maximum tip displacement [20, 24, 25]. For all nanoindentation tests, a force function with constant loading and unloading rates, each with a 5 s duration, was used. The setpoint force was set to 2  $\mu\text{N}$  when engaging the tip with the sample surface.

Friction tests were performed to obtain coefficient of friction data. The contact force was increased at a loading rate of 20  $\mu\text{N}/\text{s}$  to a maximum load, which ranged between 20 and 640  $\mu\text{N}$  and remained constant for a duration of 10 s, then the contact force was decreased to zero at a constant unloading rate of -20  $\mu\text{N}/\text{s}$ . The sliding speed and lateral displacement was set to 0.33  $\mu\text{m}/\text{s}$  and 10  $\mu\text{m}$ . The distance between sliding tracks was greater than 1  $\mu\text{m}$ . For each scratching test, 300 data sets consisting of normal and lateral force and displacement were recorded. In each set, friction force and normal displacement values were calculated as the averages of ten measurements. The coefficient of friction was determined as the ratio of the measured friction force to the applied normal force. A steady-state coefficient of friction was defined as the average of the measured coefficient of friction values in the final 7  $\mu\text{m}$  of the scratch track. All tests were repeated in at least five different locations on each deposited film examined to obtain a statistical average and ensure reproducibility.

### 2.2.2 Surface characterization

The film topography was studied using  $2 \times 2 \mu\text{m}^2$  surface area images obtained with an AFM (Veeco Metrology Group Digital Instruments Dimension 3100  $\text{\textcircled{R}}$ ). Conical silicon tips (Aspire  $\text{\textcircled{R}}$  CT300-10) with a nominal radius  $\leq 10$  nm were used in tapping mode at an approximate resonant frequency of 300 kHz and a scanning speed of  $2 \mu\text{m}/\text{s}$ . To obtain a statistical distribution of roughness data for each type of film, five different surface locations were scanned.

# Chapter 3

## Results

### 3.0.3 Roughness

The average roughness of both FCVA and RF sputtered films is shown in Figure 3.1. Representative surface roughness images of each FCVA and RF film are shown in Figure 3.2 and Figure 3.3, respectively. The average roughness of RF sputtered films decreases from 0.194 nm to 0.188 nm as the film thickness increases from 5 to 20 nm and then increases to 0.214 nm at a film thickness of 35 nm. The average roughness of FCVA films decreases from 0.131 nm to 0.123 nm as the film thickness increases from 5 to 10 nm, and then increases to 0.173 nm as the film thickness increases from 10 nm to 35 nm.

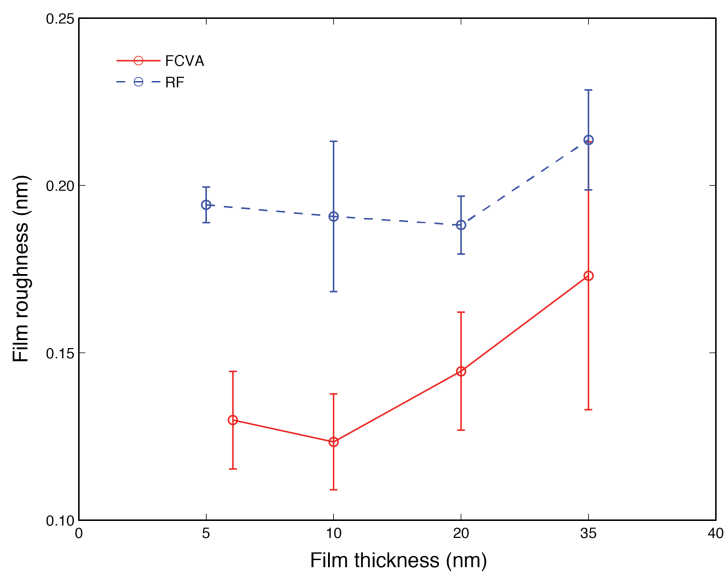


Figure 3.1: Surface roughness of FCVA and RF sputtered films of varying thickness.

### 3.0.4 Coefficient of Friction

The coefficient of friction of both FCVA and RF sputtered films for a range of normal loads across a  $10 \mu\text{m}$  scratching distance is shown in Figure 3.4. The majority of the films approach a steady-state coefficient of friction after a short sliding distance of  $\sim 2 \mu\text{m}$ , demonstrating greater variation for applied loads.

The steady-state coefficient of friction versus load is shown in Figure 3.5. A notable dip in the coefficient of friction with increasing load can be observed for all films, excluding the thinnest films (5 - 7 nm), and is more pronounced for thicker films, regardless of deposition method.

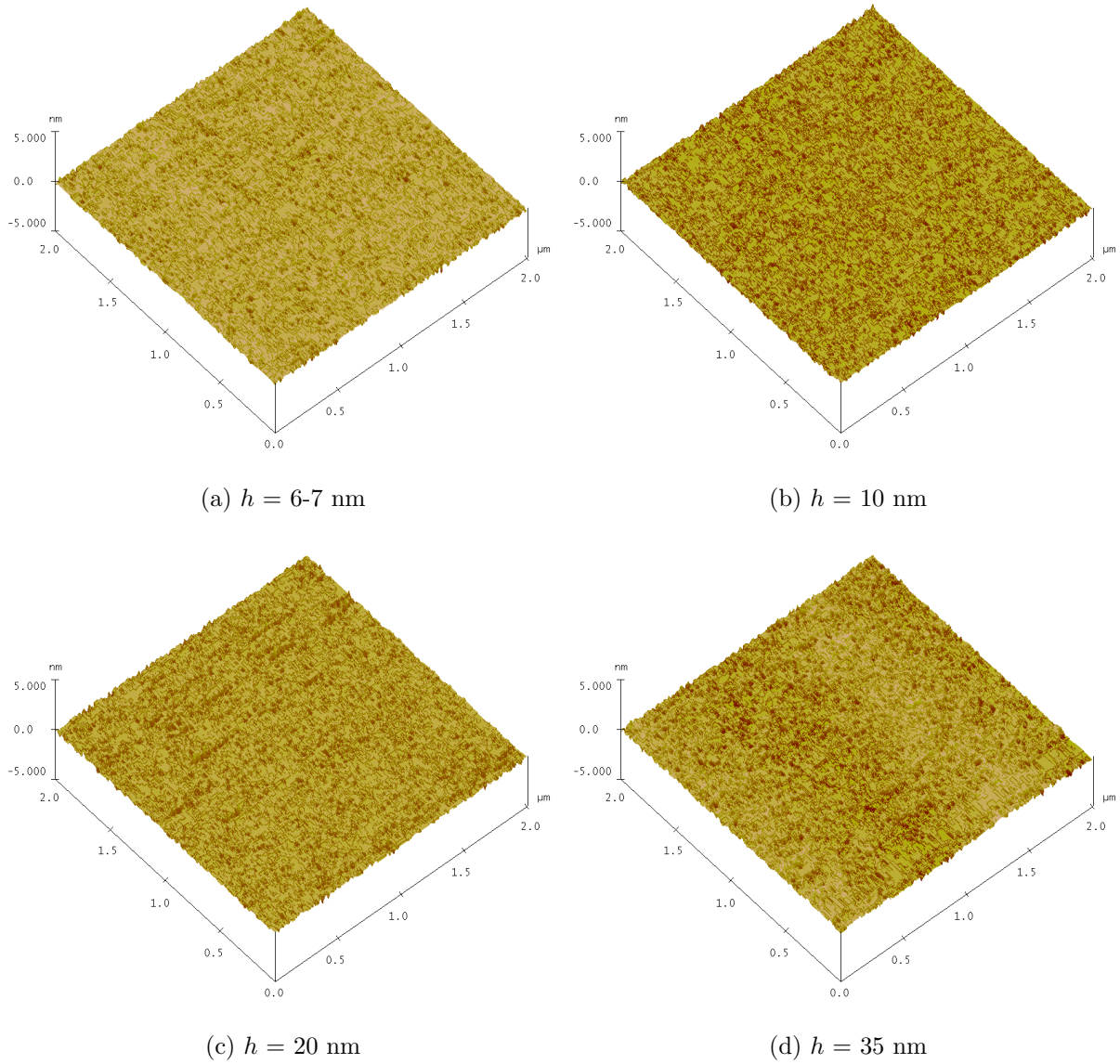


Figure 3.2: Roughness profiles of FCVA deposited films with thickness (a) 6-7 nm, (b) 10 nm, (c) 20 nm, and (d) 35 nm.

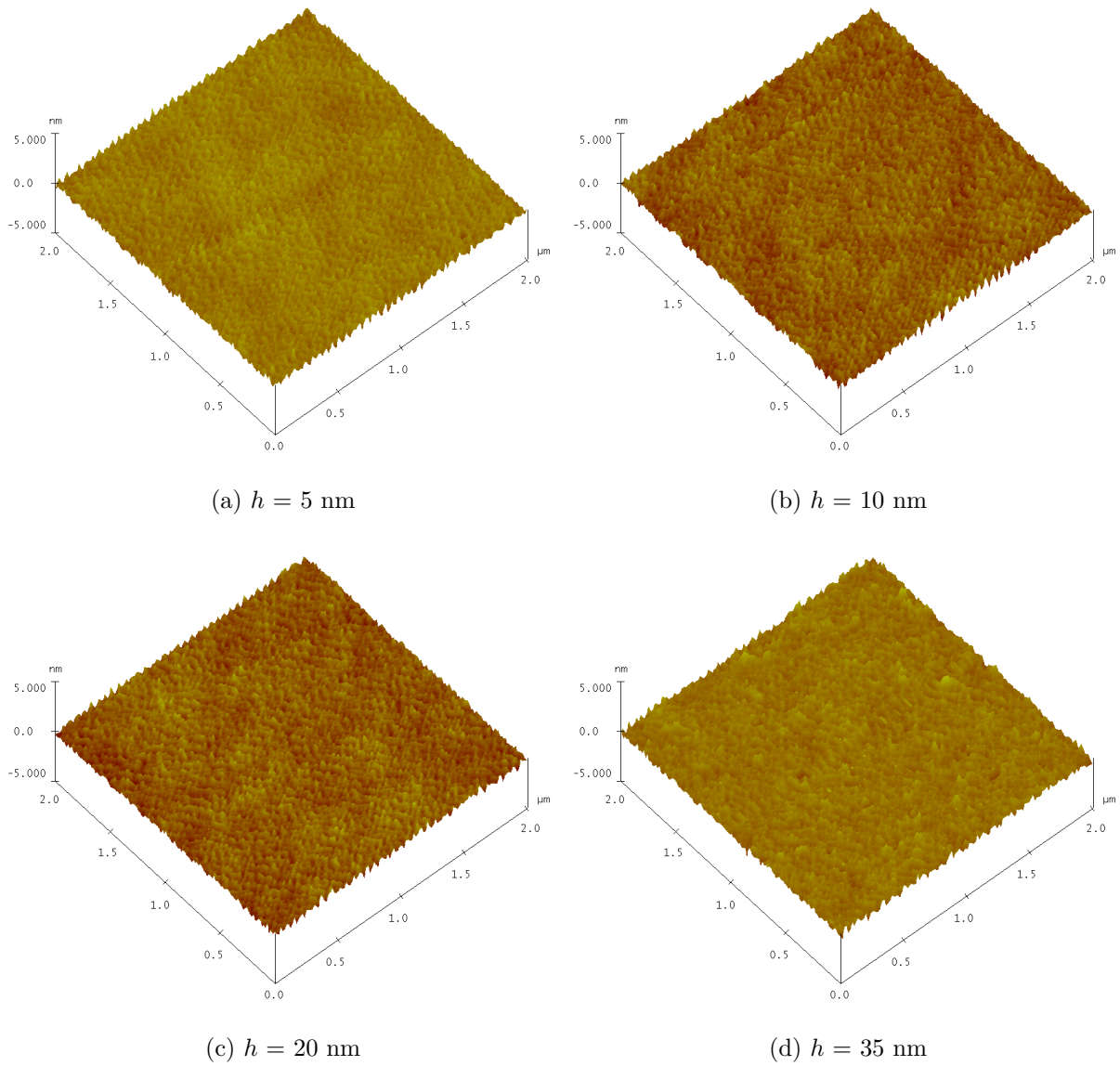


Figure 3.3: Roughness profiles of RF deposited films with thickness (a) 5 nm, (b) 10 nm, (c) 20 nm, and (d) 35 nm.

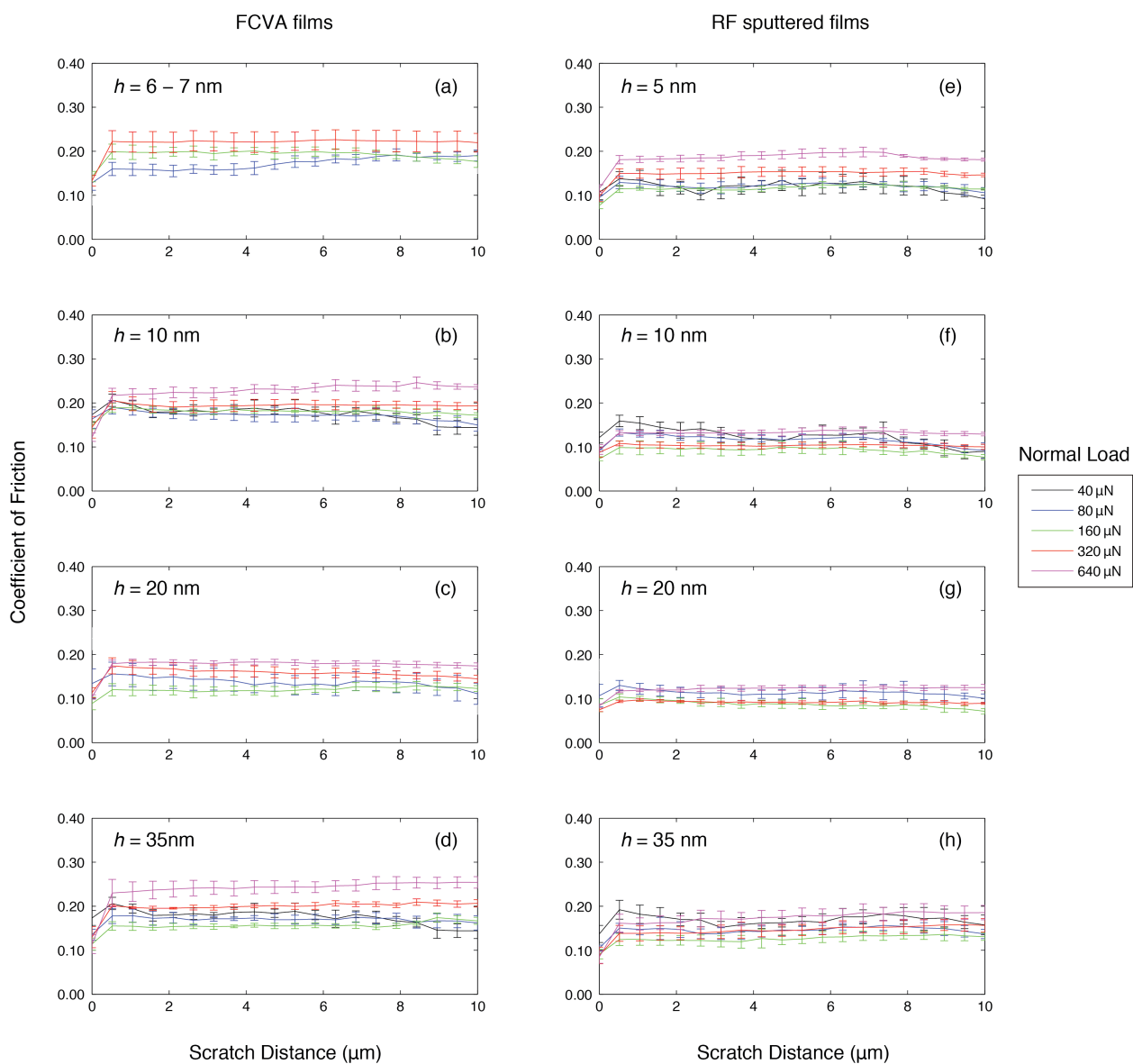


Figure 3.4: Coefficient of friction across a 10  $\mu\text{m}$  scratch track for FCVA films of thickness (a) 5 - 7 nm, (b) 10 nm, (c) 20 nm, and (d) 35 nm, and RF sputtered films with thickness, (e) 5 - 7 nm, (f) 10 nm, (g) 20 nm, and (h) 35 nm.



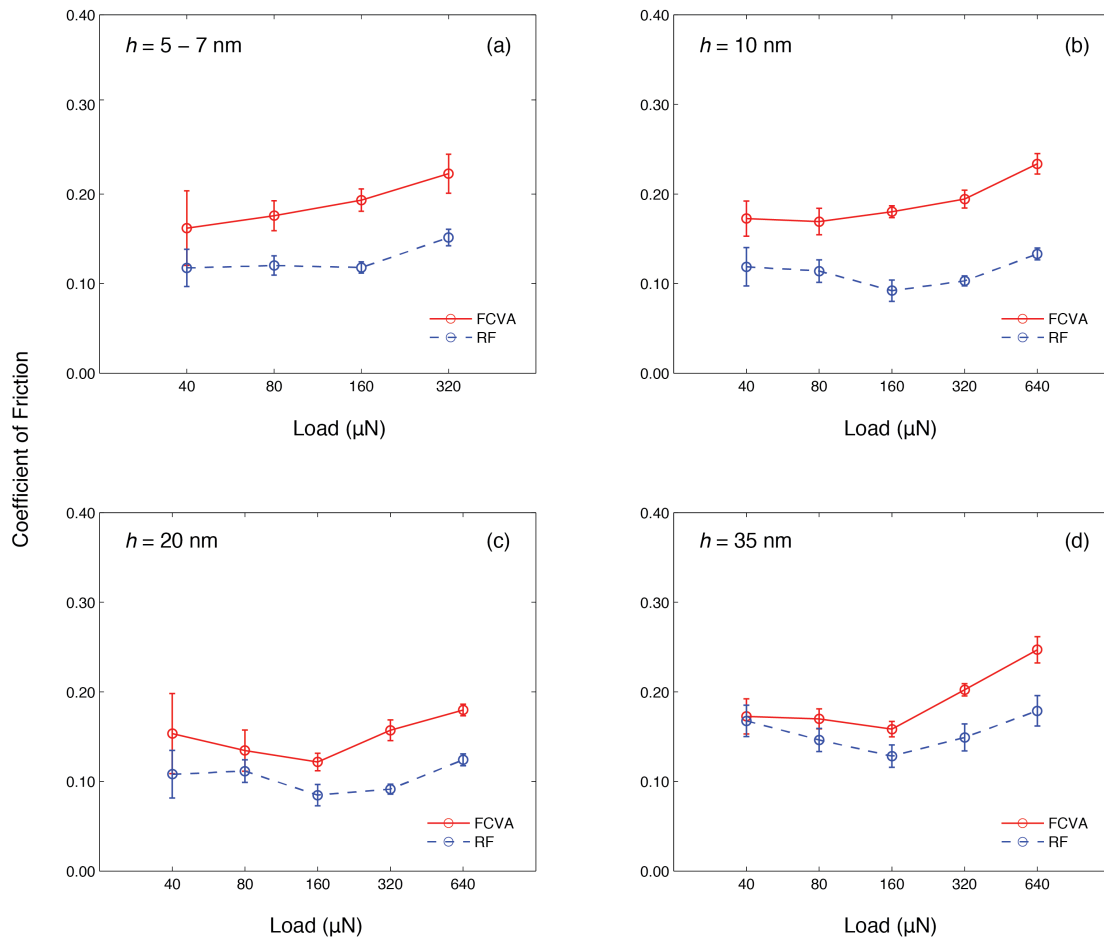


Figure 3.5: Steady state coefficient of friction for various loads for FCVA and RF sputtered films with thickness (a) 5 - 7 nm, (b) 10 nm, (c) 20 nm, and (d) 35 nm.

# Chapter 4

## Discussion

A comparison of the coefficients of friction of FCVA and RF films, shown in Figure 3.5, demonstrates several notable trends. First, the steady-state coefficient of friction of the RF films is lower than that of the FCVA films for all loads and film thicknesses. Second, most films, except those with thickness of 5-7 nm, demonstrate a decrease followed by subsequent increase in coefficient of friction with increasing load. Such phenomena may be explained by examining the elemental composition of each sublayer comprising the films, the bonding types in each layer, and the interaction between the scratching tip and the film materials including the depth of penetration and associated tribological mechanisms.

The distribution of carbon atom bonding types in the films greatly influence the tribological behavior as different hybridization modes yield different mechanical properties. Trigonal planar ( $sp^2$ ) hybridization, which imparts graphite-like behavior is softer than tetrahedral ( $sp^3$ ) hybridization which results in diamond-like behavior. An increase in  $sp^2$  content may

thus produce lower friction due to the predominantly graphitic structure of the film and act as a lubricating layer. When comparing RF and FCVA films, this is seen to be the case for RF films, which have higher concentrations of  $sp^2$  bonding and consistently exhibit lower coefficient of friction than FCVA films. The differences in shear resistance (plastic flow) may thus account for the main differences in friction properties of the RF sputtered and FCVA-deposited films despite the RF sputtered films higher roughness. Comparing coefficient of friction under different loads among the same films, however, poses a greater challenge as more tribological mechanisms must be considered.

Depending on the depth of penetration, different concentrations of  $sp^2$  and  $sp^3$  bonding exist, which influence the observed mechanical behavior. A recent study by Wang. et. al [23] revealed the structure of ultrathin  $a$ -C films synthesized by FCVA deposition using TEM, EELS, and XPS analysis, including the distribution of bonding types between each sublayer of the film. A four-layer film structure was observed comprising an interface (intermixing) layer consisting of C, Si, and, possibly, SiC, a buffer layer with continuously increasing  $sp^3$  fraction, a bulk film layer of high and constant  $sp^3$  concentration, and an ultrathin surface layer rich in  $sp^2$  hybridization. The interface layer exhibits relatively low  $sp^3$  fraction due to the low carbon concentration because carbon intermixes with Si and possible formation of SiC. The buffer layer is a thin layer of pure carbon on top of the interface layer. The  $sp^3$  fraction in that layer significantly increases towards the interface with the bulk film. When the film thickness exceeds the penetration range of  $C^+$  ions, only carbon bonding is present and compressive stresses due to the subplantation effect tend to result in  $sp^3$  hybridization,

leading to a region (bulk film) with high and constant  $sp^3$  fraction. The final impinging  $C^+$  ions results in a surface layer with increased  $sp^2$  content due to the decrease in bombardment and the associated compressive stress. An analogous trend in bonding distribution can be found in RF deposited films, where higher concentration of  $sp^3$  content are found in the bulk layer [26], though the overall  $sp^3$  concentration will be less than that of FCVA films. Considering the lighter loads first, the scratching tip penetrates the thin soft graphitic ( $sp^2$  dominant) layer and results in initially higher coefficient of friction. When the load increases up to a certain point, the frictional resistance decreases because the graphitic surface layer acts as a solid lubricant. Further penetration, however, results in plowing of the  $sp^2$  rich surface layer and an increase in shear resistance due to the  $sp^3$  bulk layer, thereby increasing the coefficient of friction. Since the substrate is also more compliant than the  $a$ -C film, the contact area increases, which also leads the contribution of adhesion and, in turn, the increase of the coefficient of friction at higher loads.

# Chapter 5

## Conclusions

An investigation of the mechanical and frictional properties of ultrathin amorphous carbon (*a*-C) films deposited on Si(100) substrates by FCVA and RF deposition methods revealed a dependence on the film's bonding type, thickness, and surface roughness. The RF sputtered films demonstrated notably lower friction than the FCVA-deposited films of equivalent thickness, possibly due to differences in shear resistance to plastic flow. The distribution in bonding types formed by each deposition method may account for the variance observed in the coefficient of friction as a function of normal load.

# References

- [1] A. Grill, “Diamond-like carbon: State of the art”. In: *Diam. Relat. Mater.* 8 (1999), pp. 428-434.
- [2] R. Hauert, “An overview on the tribological behavior of diamond-like carbon in technological and medical applications”. In: *Tribol. Int.* 37 (2004), pp. 991-1003.
- [3] J. Robertson “Diamond-like amorphous carbon”. In: *Mater. Sci. Eng. R* 37 (2002), pp. 129-281.
- [4] M. H. Kryder, E. C. Cage, T. W. McDaniel, W A. Challener, R. E. Rottmayer, G. Ju, Y. T. Hsia, and M.F. Erden. “Heat assisted magnetic recording”. In: *Proc. IEEE* 96 (2008), pp. 1810-1835.
- [5] N. Yasui, H. Inaba, K. Furusawa, and M. Saito, and N. Ohtake. “Characterization of head overcoat for 1 Tb/in magnetic recording”. In: *IEEE Trans. Magn.* 45 (2009), pp. 805-809.

- [6] N. Wang and K. Komvopoulos. "Incidence Angle Effect of Energetic Carbon Ions on Deposition Rate, Topography, and Structure of Ultrathin Amorphous Carbon Films Deposited by Filtered Cathodic Vacuum Arc". In: *Magnetics, IEEE Transactions* 48 (2012), pp. 2220-2227
- [7] J. Diaz, G. Paolicelli, S. Ferrer, and F. Comin. "Separation of the  $sp^3$  and  $sp^2$  components in the C1s photoemission spectra of amorphous carbon films". In: *Phys. Rev. B* 54 (1996), 80648069
- [8] D. R. McKenzie. "Tetrahedral bonding in amorphous carbon". In: *Rep. Prog. Phys.* 59 (1996), pp. 1611-1664.
- [9] O. R. Monteiro. "Thin film synthesis by energetic condensation". In: *Ann. Rev. Mat. Sci.* 31 (2001), pp. 111-137.
- [10] I. G. Brown. "Cathodic arc deposition of films". In: *Annu. Rev. Mater. Sci.* 28 (1998), pp. 243-269.
- [11] A.A. Voevodin and M.S. Donley. "Preparation of amorphous diamond-like carbon by pulsed laser deposition: A critical review". In: *Surf. Coat. Technol* 82 (1996), pp. 199-213.
- [12] M. K. Fung, K. H. Lai, C. Y. Chan, I. Bello, C. S. Lee, S. T. Lee, D. S. Mao, and X. Wang. "Mechanical properties and corrosion studies of amorphous carbon on magnetic disks prepared by ECR plasma technique". In: *Thin Solid Films* 368 (2000), pp. 192-202.

- [13] D. Wan and K. Komvopoulos. “Probabilistic analysis of tetrahedral carbon hybridization in amorphous carbon films”. In: *Appl. Phys. Lett.* 88 (2006), 221908(1)221908(3).
- [14] B.K. Gupta and B. Bhushan. “Mechanical and tribological properties of hard carbon coatings for magnetic recording heads”. In: *Wear* 190 (1995), pp. 110-122.
- [15] Y. Catherine. *Diamond and Diamond-like Films and Coatings*. Ed. by R.E. Clausing et al. Springer US, 1991, pp. 193-227.
- [16] J. J. Cuomo, D. L. Pappas, J. Bruley, J. P. Doyle, and K. L. Seagner. “Vapor deposition processes for amorphous carbon films with  $sp^3$  fractions approaching diamond”. In: *J. Appl. Phys.* 70 (1991), pp. 1706-1711.
- [17] B. Bhushan. *Nanotribology and Nanomechanics An Introduction*. Ed. by B. Bhushan. Springer, 2008.
- [18] F. M. Kimock, D. W. Brown, S. J. Finke, E. G. Thear. “The Evolution of Ion-Beam Diamond-like-Carbon Technology into Data Storage: Space propulsion, Sunglasses, Sliders, and now Disks”. In: *Diamonex Inc.* (Accessed 2013).
- [19] C. Donnet and A. Erdemir. *Tribology of Diamond-like Carbon Films: Fundamentals and Applications*. Springer, 2007.
- [20] W. Lu. and K. Komvopoulos. “Nanotribological and Nanomechanical Properties of Ultrathin Amorphous Carbon Films Synthesized by Radio Frequency Sputtering”. In: *Journal of Tribology*. 123 (2001), pp. 641-650.



- [21] H. S. Zhang and K. Komvopoulos. "Direct-current cathodic vacuum arc system with magnetic-field mechanism for plasma stabilization." In: *Review of Scientific Instruments* 79 (2008).
- [22] N. Wang and K. Komvopoulos. "The multilayered structure of ultrathin amorphous carbon films synthesized by filtered cathodic vacuum arc deposition". In: *J. Mater. Res.* 28 (2013), pp. 2124-2131.
- [23] H. S. Zhang and K. Komvopoulos. "Surface modification of magnetic recording media by filtered cathodic vacuum arc". In: *Journal of Applied Physics* 106 (2009).
- [24] J. Endrino, R. Escobar, R. Galindo, H. S. Zhang, M. Allen, R. Gago, A. Espinosa, and A. Anders. "Structure and properties of silver-containing a-C(H) films deposited by plasma immersion ion implantation". In: *Surface and Coating Technology*. 202 (2008), pp. 3675-3682.
- [25] W. Lu, K. Komvopoulos, P. Patsalas, C. Charitidis, M. Gioti, and S. Logothetidis. "Microstructure and Nanomechanical and Optical Properties of Single and Multi-Layer Carbon Films Synthesized by Radio Frequency Sputtering." In: *Surface and Coatings Technology* 168 (2003), pp. 12-22.
- [26] D. Wan and K. Komvopoulos. "Transmission electron microscopy and electron energy loss spectroscopy analysis of ultrathin amorphous carbon film". In: *J. Mater. Res.* 19 (2004), pp. 2131-2136.

DEPARTMENT OF MECHANICAL ENGINEERING

UNIVERSITY OF CALIFORNIA - BERKELEY

\*\*\*\*\*

LIBRARY PERMISSION FORM

MASTER'S PLAN II

Last Name:  First Name:  Middle Name:   
SID:  Major Field Area:  Degree Goal:   
Phone Number:  Email:  Submission Date:

Report Title:

IMMEDIATE RELEASE

I authorize the Department of Mechanical Engineering to release my report to the UC Berkeley Library and have it made available to the public electronically through the library catalog as soon as is feasible after my report has been filed.

EMBARGO FOR 2 YEARS

I wish my report to be withheld for 2 years following the date of filing after which time it will be released to the UC Berkeley Library and made available to the public electronically through the library catalog.

EMBARGO FOR LESS/MORE THAN 2 YEARS

I wish my report to be withheld for \_\_\_\_\_ year(s) following the date of filing after which time it will be released to the UC Berkeley Library and made available to the public electronically through the library catalog.

Explanation required if more than 2 years:

Student Signature: Jozef Matlak Date: 5/15/14  
MS Committee Chair Signature: [Signature] Date: 5/15/14